Growing unstable manifolds of planar maps

Bernd Krauskopf
Theoretical Physics
Free University
De Boelelaan 1081
1081 HV Amsterdam
The Netherlands
berndk@nat.vu.nl

Hinke Osinga
The Geometry Center
University of Minnesota
400 Lind Hall
Minneapolis, MN 55455
U.S.A.
hinke@geom.umn.edu

September 1997

Abstract

We present a new method for computing the global one-dimensional unstable manifold of a hyperbolic fixed point of a map. The key idea is to 'grow' the manifold, where the speed of growth is determined only by the curvature of the manifold, and not by the dynamics. In other words, we do not use the standard approach of iterating a fundamental domain. Furthermore, we present two new families of planar maps, that we feel are useful for testing any method for computing unstable manifolds. The performance of our algorithm is illustrated with these two maps, and with the Poincaré map of the driven-damped pendulum.

1 Introduction

Many interesting dynamical systems can be described by a map from a given state space to itself. Time is thought to be discrete, and the map describes the evolution of a state of the system by iteration. An important class are *planar diffeomorphisms*, that is, differentiable maps on $\mathbb{R}^2$ with differentiable inverses. Well-known examples are either explicitly defined, like the Hénon map [8] and the Ikeda map [11, 7], or Poincaré maps of three-dimensional vector fields, like those of the forced Van der Pol and Duffing oscillators [6]. Planar diffeomorphisms may have very complicated dynamics. Their global behavior is organized by the stable and unstable manifolds of the saddle points. These manifolds are one-dimensional curves (often of infinite arclength) that can have extremely complicated embeddings into the plane. For example, a transverse intersection of stable and unstable manifolds leads to homoclinic or heteroclinic tangle with horseshoe dynamics [18]. Furthermore, stable manifolds form boundaries between different attractors, and their bifurcations can lead to discontinuous changes of the attractor [5, 7]. Stable and unstable manifolds are global objects that usually cannot be found analytically, but need to be computed numerically.

To keep the exposition simple, we stay in the context of planar diffeomorphisms. In this setting the only invariant set of saddle type with stable and unstable manifolds is a saddle point. Suppose that we are given an orientation preserving diffeomorphism $f : \mathbb{R}^2 \to \mathbb{R}^2$. (This is not a restriction: if f is orientation reversing consider its second iterate.) Let x_0 be a saddle point of f. Hence, $f(x_0) = x_0$ and the Jacobian $Df(x_0)$ has two real eigenvalues λ^s and λ^u with $0 < \lambda^s < 1 < \lambda^u$. The unstable manifold of x_0 is defined as

$$W^u(x_o) \;:=\; \{x \in \mathbb{R}^2 \mid f^{-n}(x) \to x_0 \text{ as } n \to \infty\},$$

where f^n denotes the n-th iterate of f. Note that, since f is a diffeomorphism, the stable manifold $W^s(x_0)$ is simply the unstable manifold of the inverse f^{-1} at x_0. This is why we only consider the unstable manifold $W^u(x_o)$ from now on. The Unstable Manifold Theorem [17] guarantees the existence of the *local unstable manifold* $W^u_{\text{loc}}(x_0)$ in a neighborhood of x_0. Furthermore, it states that $W^u_{\text{loc}}(x_0)$ is tangent to the unstable eigenspace $E^u(x_0)$ of λ^u.

The idea behind most algorithms is to globalize the local unstable manifold $W^u_{\text{loc}}(x_0)$ by *iterating a fundamental domain*. Pick a point $p \in W^u_{\text{loc}}(x_0)$ at some small distance from x_0. Then the piece of $W^u_{\text{loc}}(x_0)$ between p and $f(p)$ is a fundamental domain F_p, meaning that all orbits on the branch of

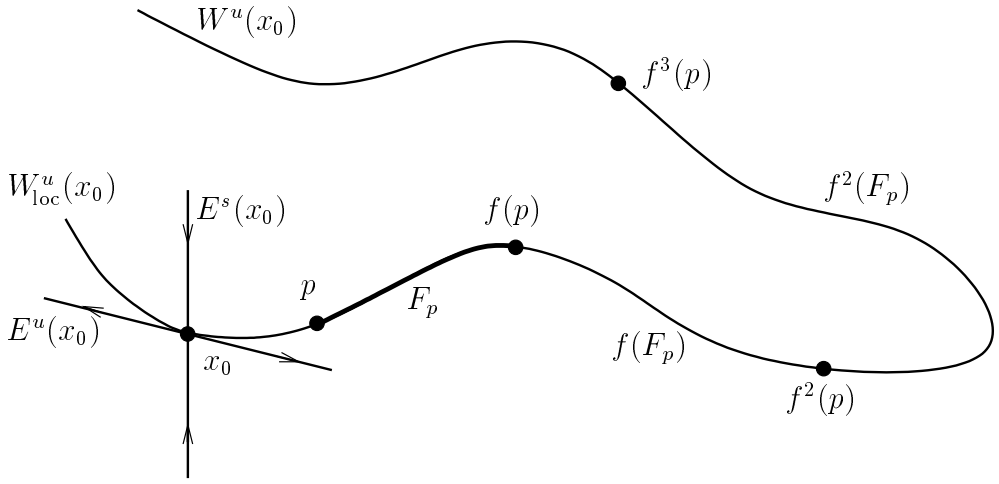

Figure 1: *Iterating a fundamental domain.*

$W^u(x_o)$ that contains p have exactly one point in F_p. In particular, the iterates of F_p will cover this branch of $W^u(x_o)$; see Fig. 1. To use this idea one needs to compute an approximation of $W^u_{\rm loc}(x_0)$ in a neighborhood of x_0. Often the linear approximation $E^u(x_0)$ suffices [23]. If needed, a higher-order approximation of $W^u_{\rm loc}(x_0)$ can be computed as a series representation [21], or by graph transform techniques [15, 10]. Note that it is not possible to iterate F_p as a continuous object, but only as a finite set of points. This results in a sequence of points approximating $W^u(x_o)$. A considerable problem is that F_p typically stretches and develops sharp folds under iteration. This is why extra points need to be added between consecutive points in the sequence when their distance or the curvature become too large. To achieve this one can work with the original fundamental domain F_p [21, 23], or with the previous iterate of F_p [19, 9].

There are some methods that do not use iteration of a fundamental domain. First, there is the *evolution of a geometric object*: a large number of points on, for example, a small circle around x_0 is iterated; see e.g. [12]. The iterates align along $W^u(x_o)$ and provide an approximation, the quality of which may be problematic unless very many points on the initial circle are iterated. Secondly, there is the computation of *straddle trajectories*, that is, backward orbits of points near $W^u(x_o)$. By determining along which branch of $W^s(x_o)$ these orbits end up one can find points on $W^u(x_o)$ by bisection [14].

Finally, there is the method of finding an *outer approximation* of $W^u(x_o)$ by rectangular cells [3, 4, 16]. An initial rectangle, where interesting dynamics is expected, is recursively subdivided into smaller cells. Only the cells containing a piece of $W^u(x_0)$ are kept until a sufficient resolution is reached. Note that the manifold is not represented as a one dimensional object in this approach.

In this paper we present a new method for the computation of the unstable manifold $W^u(x_0)$. It is described in detail in Section 2. We compute a sequence of points on $W^u(x_0)$, and the manifold itself is represented by piecewise linear interpolation as the set of line segments between consecutive points. We choose a suitable point p near x_0 on the linear approximation $E^u(x_0)$ of $W^u_{\rm loc}(x_0)$. Our initial sequence is then $\{x_0, p\}$. The key idea is to grow the manifold in steps by adding a single point on $W^u(x_0)$ to the sequence at each step. To do so we first find an appropriate steplength Δ by monitoring the curvature. Then we look for a preimage, that is, a point q in one of the line segments so that $f(q)$ is at (approximately) distance Δ from the last point of the sequence; see Fig. 2. This can be done by first determining the correct line segment L, and then finding $q \in L$ by bisection. (We allow the distance between $f(q)$ and the last point to be in a small interval around Δ to cut down the number of bisection steps for finding q.) Finally, $f(q)$ is added to the sequence and the step is complete. The algorithm stops when the manifold is computed up to a prescribed arclength.

Notice that we do not use the idea of iterating a fundamental domain. Instead we grow the manifold with a speed that is determined only by the curvature of the manifold and not by the dynamics. At the same time we obtain the parametrization of $W^u(x_0)$ by arclength. We remark that it is possible to use a higher order approximation to $W^u_{\rm loc}$ and higher order interpolation between consecutive points, for example splines. However, linear approximation is fast in practice and also sufficient, provided the parameters defining the quality are small enough; see Section 2.2. Our method also works for the computation of one-dimensional unstable manifolds in higher-dimensional spaces. We finally remark that the idea of growing the manifold in steps of Δ is used in [13] to compute two-dimensional manifolds of diffeomorphisms on $\mathbb{R}^3$.

A second goal of this paper is to propose two new maps that are in some sense ideal for testing purposes. The *shear map* features a tangency to a piece of manifold that is in fact linear, and the *IBV map* models two independent blinking vortices and has very complicated recursive spiraling of manifolds.

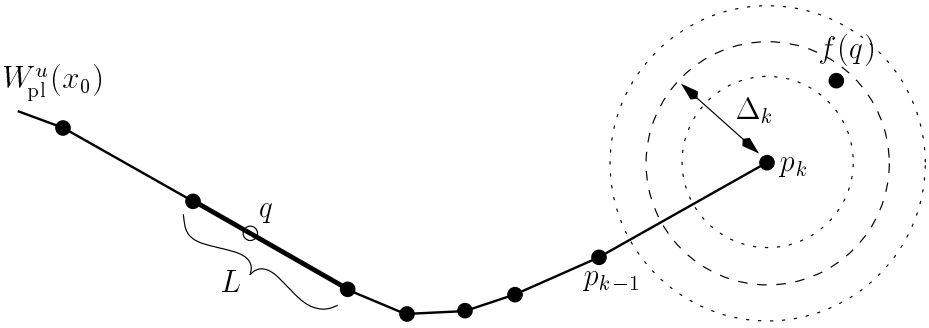

Figure 2: *The next point $p_{k+1} = f(q)$ is chosen at (approximately) distance Δ_k from p_k.*

Our algorithm is tested with these explicit maps and with the Poincaré map of the driven-damped pendulum in Section 3.

2 The algorithm

Our algorithm for computing one-dimensional stable and unstable manifolds is based on the algorithm for two-dimensional manifolds described in [13]. We start with a linear approximation of the local unstable manifold and grow the manifold with a speed depending on the curvature, up to a prespecified arclength l.

Recall that $f : \mathbb{R}^2 \to \mathbb{R}^2$ is an orientation preserving diffeomorphism with a saddle point $f(x_0) = x_0$. The algorithm produces a list $M = \{p_0, p_1, \ldots, p_N\}$ of mesh points on the unstable manifold $W^u(x_0)$ starting with the fixed point $p_0 = x_0$ and the point p_1 at a small distance δ from x_0 in the unstable eigenspace $E^u(x_0)$. The total number N of points is variable and depends on the accuracy of the computation and the arclength l. During the computation we need the *continuous object* $W^u_{\rm pl}(x_0)$, which is the piecewise linear approximation of the computed part of $W^u(x_0)$ formed by the line segments between consecutive mesh points. Initially, $W^u_{\rm pl}(x_0)$ is the interval $[p_0, p_1]$, that is, it is the linear approximation of $W^u_{\rm loc}(x_0)$. As we grow the manifold, points are added to M in steps, and $W^u_{\rm pl}(x_0)$ changes accordingly. The complete algorithm is shown in pseudo-code in Fig. 4.

We now describe a single step and suppose that $M = \{p_0, p_1, \ldots, p_k\}$ is

already known. The next point p_{k+1} should have the property that the line segment $[p_k, p_{k+1}]$ accurately approximates $W^u(x_0)$. Hence, the curvature of $W^u(x_0)$ determines the allowed distance between p_k and p_{k+1}. The idea is to use a guess Δ_k for this distance, which is adapted according to the curvature; see the next section for the details. Using the estimate Δ_k, we want to find p_{k+1} in a small annulus around the circle centered at p_k with radius Δ_k; see Fig. 2. To this end, we search in $W^u_{\rm pl}(x_0)$ for the line segment L that is mapped by f to a curve which intersects the circle with center p_k and radius Δ_k. We start this search with the line segment in $W^u_{\rm pl}(x_0)$ that contains the preimage of p_k and move linearly through $W^u_{\rm pl}(x_0)$. Once L is found, we use bisection to find a point $q \in L$ such that

$$(1-\varepsilon)\Delta_k < \| f(q) - p_k \| < (1+\varepsilon)\Delta_k .$$

The uncertainty factor ε is used to reduce the number of bisection steps. Troughout all computations we chose the fixed value $\varepsilon = 0.2$.

The point $p_{k+1} = f(q)$ is a candidate for the next point in M. We now check whether the interpolation error between the line segment $[p_k, p_{k+1}]$ and $W^u(x_0)$ is within the desired accuracy. This depends on the local curvature of $W^u(x_0)$ and is explained in the next section. If $[p_k, p_{k+1}]$ is acceptable then p_{k+1} is added to M, $[p_k, p_{k+1}]$ is added to $W^u_{\rm pl}(x_0)$, and the step is complete. However, it is possible that Δ_k was too large an estimate for the allowed distance. Then we reject p_{k+1}, half the estimate Δ_k, and repeat the process.

Remark 1 *It may not be possible to find a point p_{k+1} at (approximately) distance Δ_k from p_k. This occurs when $W^u(x_0)$ is of finite arclength, hence, $W^u(x_0)$ is attraced to a point attractor. In this situation we also half Δ_k and try again.*

2.1 Mesh adaptation

We say that $W^u_{\rm pl}(x_0)$ accurately approximates $W^u(x_0)$ if the maximal error $\varepsilon_{\rm pl}$ between $W^u_{\rm pl}(x_0)$ and the corresponding first finite piece of $W^u(x_0)$ is small. The error $\varepsilon_{\rm pl}$ depends on the distances Δ_k between consecutive mesh points. In order to keep the interpolation error on the linear line segment of $W^u_{\rm pl}(x_0)$ small the allowed distance between mesh points must be adapted to the local curvature of $W^u(x_0)$. If $W^u(x_0)$ is locally almost a straight line, only a few mesh points are required, whereas many points are needed where $W^u(x_0)$ has sharp folds.

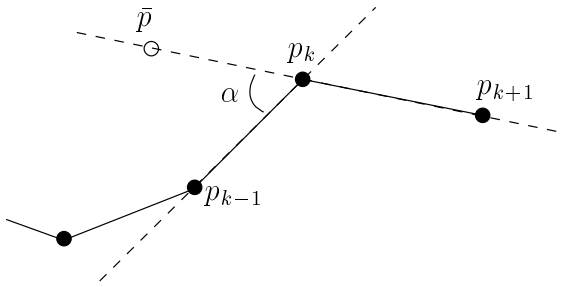

Figure 3: *In determining the accuracy of the computation we use the angle α formed by the three successive points p_{k-1}, p_k and p_{k+1}.*

The distribution of points on the manifold is monitored with a method based on the technique in [9]. Assume that we have found a candidate p_{k+1} in a small annulus around the circle with center p_k and radius Δ_k. We need to check whether Δ_k is an allowable distance. To determine this, we consider the angle α between the lines through p_{k-1}, p_k and p_k, p_{k+1}, as sketched in Fig. 3. This angle is approximated as follows. Figure 3 indicates that

$$\sin\left(\frac{\alpha}{2}\right) = \frac{\|\bar{p} - p_{k-1}\|}{2\,\|p_k - p_{k-1}\|},$$

where

$$\bar{p} = p_k + (p_k - p_{k+1}) / \|p_k - p_{k-1}\| \,. \tag{1}$$

Since $\sin\left(\frac{\alpha}{2}\right) \approx \frac{\alpha}{2}$ if α is small, we simply use the approximation

$$\alpha_k = \frac{\|\bar{p} - p_{k-1}\|}{\|p_k - p_{k-1}\|}. \tag{2}$$

We remark that Hobson [9] does not use p_{k-1} for the computation of α_k, but has a so-called reference point instead, which can be considered as an estimate for the future point p_{k+2}. The adaptation works by checking the conditions

$$\begin{array}{rcccl} \alpha_{\min} & < & \alpha_k & < & \alpha_{\max} \\ (\Delta\alpha)_{\min} & < & \Delta_k\alpha_k & < & (\Delta\alpha)_{\max}, \end{array} \tag{3}$$

where the bounds are four prespecified control parameters; compare [9]. The first condition states that α_k should be small, which will avoid that the algorithm cuts off edges in sharp folds. The second condition controls the local interpolation error.

Algorithm GLOBALIZE1D

Input:	f, x_0, v,	$f(x_0) = x_0$, $E^u(x_0) = \mathrm{span}(v)$;
	δ,	initial distance from x_0;
	Δ,	first estimate for Δ_k;
	$\alpha_{\min}$, $\alpha_{\max}$, $(\Delta\alpha)_{\min}$, $(\Delta\alpha)_{\max}$,	tolerances for α_k and $\Delta_k\alpha_k$;
	l_{arc},	total arclength to be computed;
Output:	M,	list of mesh points;

M	**list** of Point;
q, p_k, p_{k+1}	**Point**;
L, L_{old}	pointer to **Point**, points to left side of line segment;
Δ_k, α_k, `arclength`	**real**;

Begin

1 ADD(M, x_0); $p_k := x_0 + \delta v$; ADD(M, p_k);
2 `arclength` $:= \delta$; $\Delta_k := \Delta$; $L := \&x_0$; $L_{\mathrm{old}} := L$;
3 **while** `arclength` $< l_{\mathrm{arc}}$ **do**
4 **while** $\| f(L \uparrow next) - p_k \| < \Delta_k$ **do**
5 $L := L \uparrow next$;
Comment: in next loop L contains the preimage of p_k
6 $q :=$ BISECT(L, Δ_k);
Comment: now $(1-\varepsilon)\Delta_k < \| f(q) - p_k \| < (1+\varepsilon)\Delta_k$
7 $p_{k+1} := f(q)$; $\alpha_k :=$ ANGLE(M, p_{k+1});
8 **if** $(\alpha_k < \alpha_{\max})$ & $(\Delta_k\alpha_k < (\Delta\alpha)_{\max})$ **then**
9 **if** $(\alpha_k < \alpha_{\min})$ & $(\Delta_k\alpha_k < (\Delta\alpha)_{\min})$ **then**
10 $\Delta_k := 2\Delta_k$;
11 `arclength` $:=$ `arclength` $+ \| p_{k+1} - p_k \|$;
12 ADD(M, p_{k+1});
13 $p_k := p_{k+1}$; $L_{\mathrm{old}} := L$;
else
14 $\Delta_k := \frac{1}{2}\Delta_k$; $L := L_{\mathrm{old}}$;
End.

Figure 4: *The algorithm* GLOBALIZE1D *in pseudo-code.*

If both $\alpha_k < \alpha_{\max}$ and $\Delta_k \alpha_k < (\Delta\alpha)_{\max}$ then the point p_{k+1} is acceptable. We use $\Delta_{k+1} = \Delta_k$ unless Δ_k is rather small, that is, when both $\alpha_k < \alpha_{\min}$ and $\Delta_k \alpha_k < (\Delta\alpha)_{\min}$. In this case, we set $\Delta_{k+1} = 2\Delta_k$. On the other hand, if $\alpha_k \geq \alpha_{\max}$ or $\Delta_k \alpha_k \geq (\Delta\alpha)_{\max}$ then p_{k+1} is not acceptable, we set $\Delta_k = \frac{1}{2}\Delta_k$ and try again. This strategy can be found implemented in pseudo-code in Fig. 4.

Remark 2 *In practice, Δ_k might become very small, typically when the manifold is about to have a very sharp fold. Therefore, we use a lower bound $\Delta_{\min}$ on Δ_k. If p_{k+1} lies at distance $\Delta_k = \Delta_{\min}$ from p_k, and still α_k is too big, either because $\alpha_k \geq \alpha_{\max}$ or because $\Delta_k \alpha_k \geq (\Delta\alpha)_{\max}$, we accept p_{k+1} and report the error. On the other hand, we do allow Δ_k to become arbitrarily large. In practice, Δ_k becomes very large when the manifold is not confined to a bounded region, in which case there are long, almost straight sections; compare the stable manifold of the shear map in Sec. 3.1.*

2.2 Discussion of the accuracy

The accuracy of a computation depends on the distribution of the mesh points and the initial distance along $E^u(x_0)$. It is standard [23] to proof that the total error $\varepsilon_{\rm pl}$ is bounded by using the bounded Lipschitz constant of f restricted to a neighborhood of x_0 that contains the computed part of the manifold. Along the lines of [23], a full proof of our method for the globalization of two-dimensional unstable manifolds is given in [13]. This proof carries over to the one-dimensional case, and we only sketch the main idea here.

The initial error between the first line segment in the linear unstable eigenspace $E^u(x_0)$ and the local unstable manifold $W^u_{\rm loc}(x_0)$ is controlled by the parameter δ, the initial distance from the fixed point x_0. Since $W^u(x_0)$ is a collection of f-images of $W^u_{\rm loc}(x_0)$, this initial error grows with the number of iterates of the line segment that are needed to cover the computed part. We get an additional error ε_I from the interpolation between the mesh points, because we grow the manifold by taking images of interpolated points. The total error $\varepsilon_{\rm pl}$ is bounded, provided ε_I is small. In [9] it is discussed that the interpolation error ε_I is controlled by keeping the product $\Delta_k \alpha_k$ small.

Remark 3 *In [23] the global manifold is obtained by iterating points from the initial line segment $[p_0, p_1]$. This means that one only needs to store*

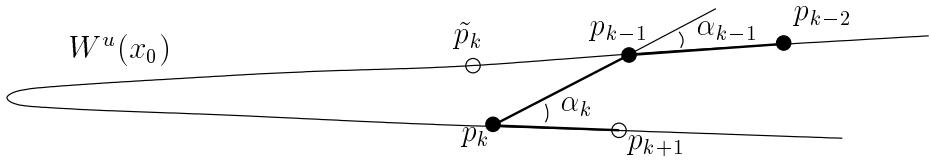

Figure 5: *A situation where part of the manifold might be missed.*

$[p_0, p_1]$, but the function must be evaluated many times. Our technique uses a more complicated datastructure, but we need less function calls; see also [9]. Furthermore, far away from x_0, two successive points p_k and p_{k+1} have preimages in $[p_0, p_1]$ that lie extremely close to each other. The algorithm in [23] stops when these preimages become equal up to computer precision. This problem occurs much later for our method.

The final issue we discuss is the problem of cutting off folds. It may seem that our algorithm cuts off sharp folds, because the point p_k might be chosen on the returning branch; see Fig. 5. The point p_k would be accepted, because $\Delta_{k-1} = \| p_k - p_{k-1} \|$ and α_{k-1} satisfy (3). However, the next angle α_k is then virtually independent of the distance between p_{k+1} and p_k, and p_{k+1} would eventually be accepted once $\| p_{k+1} - p_k \| \leq \Delta_{min}$.

Note that an early jump to the returning branch can only occur when the preimage of the fold between p_{k-1} and p_k comes from a single interval. As the manifold grows, at first only mild folds appear. These mild folds map to longer and sharper folds; see for example Fig. 6. In the computation, mild folds are certainly followed properly by the algorithm, and near the mild fold there is already a relatively large number of intervals. The number of intervals in the approximation only grows for the next, larger and sharper folds. This means that the preimage of a sharp fold never lies entirely in a single interval. In other words, first the other candidate $\tilde{p}_k$ before the fold is found, and the fold is not missed; see Fig. 5.

3 Examples

In this section we propose two planar maps, the shear map and the IBV map, that we feel are ideal for testing any algorithm for the computation of

global (un)stable manifolds. The shear map has homoclinic tangencies to a segment of the coordinate axes, and the IBV map is characterized by strong recursive spiraling. We demonstrate the performance of our algorithm with these two maps and with the Poincaré map of the driven-damped pendulum.

3.1 The shear map

In this section we introduce the *shear map*, a one-parameter family of diffeomorphisms on $\mathbb{R}^2$, with the following special properties. The origin is always a saddle point and the stable and unstable manifolds contain parts of the coordinate axes. Furthermore, the family has a first homoclinic tangency for a particular parameter value. In other words, near the origin one of the manifolds involved in the tangency is known: it is a part of a coordinate axis, and one can simply check if the other manifold returns tangent to this axis.

The idea of the shear map is from [18], where it is used to obtain a simple example of a map with intersecting stable and unstable manifolds. We start with the linear map

$$\phi \begin{pmatrix} x \\ y \end{pmatrix} = \begin{pmatrix} \lambda^u x \\ \lambda^s y \end{pmatrix},$$

where $0 < \lambda^s \leq (\lambda^u)^{-1} < 1$ are fixed. Clearly, the origin $\mathbf{0}$ is a saddle point of ϕ and its stable and unstable manifolds are the coordinate axes. Consider now the one-parameter family of maps

$$\psi_c \begin{pmatrix} x \\ y \end{pmatrix} = \begin{pmatrix} x - c\, f(x+y) \\ y + c\, f(x+y) \end{pmatrix},$$

where

$$f(z) = \begin{cases} 0 & \text{for} \quad z \leq 1 \\ (z-1)^2 & \text{for} \quad z > 1 \ . \end{cases}$$

The map ψ_c shears the plane, because it is a drift of magnitude $\sqrt{2}\ c\, f(x+y)$ along the diagonal lines $\{(x,y) \mid x + y = const > 1\}$. The shear map is now defined as the compositon

$$\Psi_c = \psi_c \circ \phi \ . \tag{4}$$

By construction of Ψ_c the origin $\mathbf{0}$ is a saddle point for any c, with eigenvalues λ^u and λ^s. Furthermore, the interval $\{x \in (-\infty, 1],\ y = 0\}$ is contained in $W^u(\mathbf{0})$, and $\{y \in (-\infty, (\lambda^s)^{-1}],\ x = 0\}$ is contained in $W^s(\mathbf{0})$.

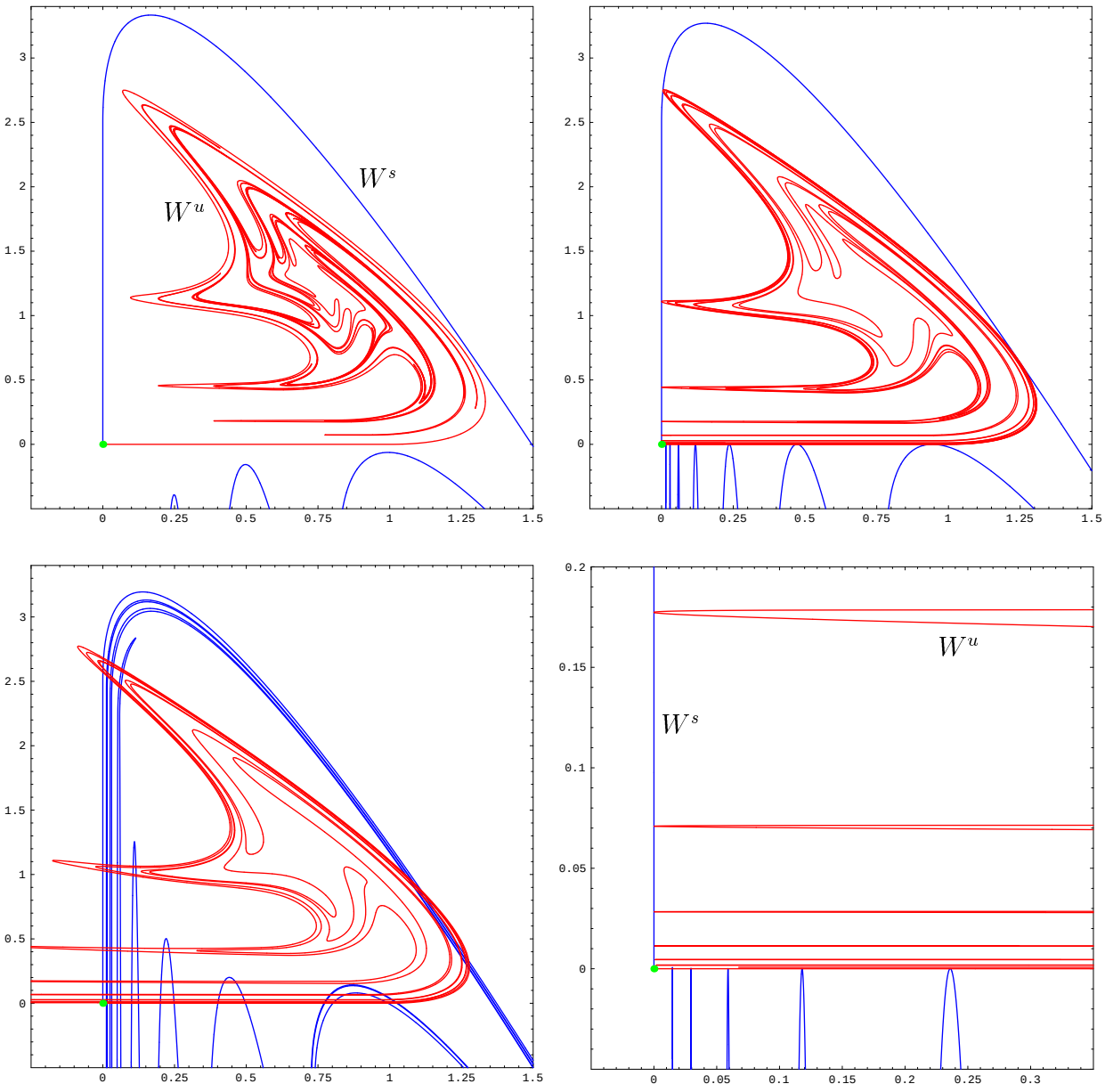

Figure 6: *The shear map before (top left), approximately at (top right), and after (lower left) the first tangency. The enlargement near the fixed point (lower right) illustrates that this tangency can be found quite accurately. ($c = 0.75$, $c = 0.811580$, $c = 0.9$, respectively; branch of $W^u(\mathbf{0})$ computed up to arclength 100, branch of $W^s(\mathbf{0})$ computed up to arclength 5,000.)*

We now show that there must be a first homoclinic tangency for a particular $c^* \in [0, \lambda^u]$. Clearly the manifolds $W^u(\mathbf{0})$ and $W^s(\mathbf{0})$ do not intersect for $c = 0$. By construction $W^u(\mathbf{0})$ contains the image of the interval $\{x \in (1, \lambda^u],\ y = 0\}$ under ψ_c. Consequently, $W^u(\mathbf{0})$ intersects the interval $\{y \in (0, (\lambda^s)^{-1}],\ x = 0\} \in W^s(\mathbf{0})$ if the right endpoint $(\lambda^u, 0)$ of the above interval gets mapped to the left of the y-axis under ψ_c. This is the case if $c \geq \lambda^u$, showing the existence of c^* by continuity.

Throughout our computations we have chosen $\lambda^s = 0.4$ and $\lambda^u = 2.0$. Figure 6 shows the interesting branches of the stable and unstable manifolds before the tangency for $c = 0.75$ (top left), approximately at the tangency for $c = 0.811580$ (top right), and after the tangency for $c = 0.9$ (lower left). The unstable branches have been computed up to arclength 100, and the stable branches up to arclength 5,000. (The stable manifolds make very long excursions into the lower half plane.) For the accuracy we have chosen $\alpha_{\min} = 0.2,\ \alpha_{\max} = 0.3,\ (\Delta\alpha)_{\min} = 10^{-6},\ (\Delta\alpha)_{\max} = 10^{-5}$ and $\Delta_{\min} = 10^{-4}$. (Recall that $\varepsilon = 0.2$ in all computations.)

Figure 6 (lower right) shows an enlargement near the origin at the approximate moment of tangency. A numerically found first tangency is never excactly a tangency. Due to the Λ-Lemma [17], this will become clearly visible for a suitable iterate, that is, when a longer piece of the manifolds is computed. Making sure that W^u and W^s have tangencies along the entire computed arclength allows one to find the value of c^* with any precision. (We found $c^* \approx 0.811580$, which is precise up to five digits.) Clearly, this also requires to compute W^u and W^s with sufficient accuracy. It is an interesting observation that looking at long pieces of W^u and W^s also allows to check the accuracy of the computed manifolds themselves. If one looks closely one notices that the last loop of W^s just intersects W^u. On the other hand, the last loop of W^u just misses W^s. The theory does not allow this phenomenon, and the fact that it occurs in the figure shows that W^u and W^s have not been computed accurately over the entire prescribed arclength. The solution is to choose a finer mesh, which would allow us to make sure that all computed tangencies lie on the coordinate axes.

To give an idea of how the mesh depends on the curvature, Figure 7 shows successive enlargements of the unstable manifold for $c = 0.811580$. The manifold was now computed up to arlength 500, and in the largest magnification (lower right) we have not connected the points of the mesh. This shows that the points are nicely distributed, but that the distance between neighboring points varies slightly because of the uncertainty factor $\varepsilon = 0.2$.

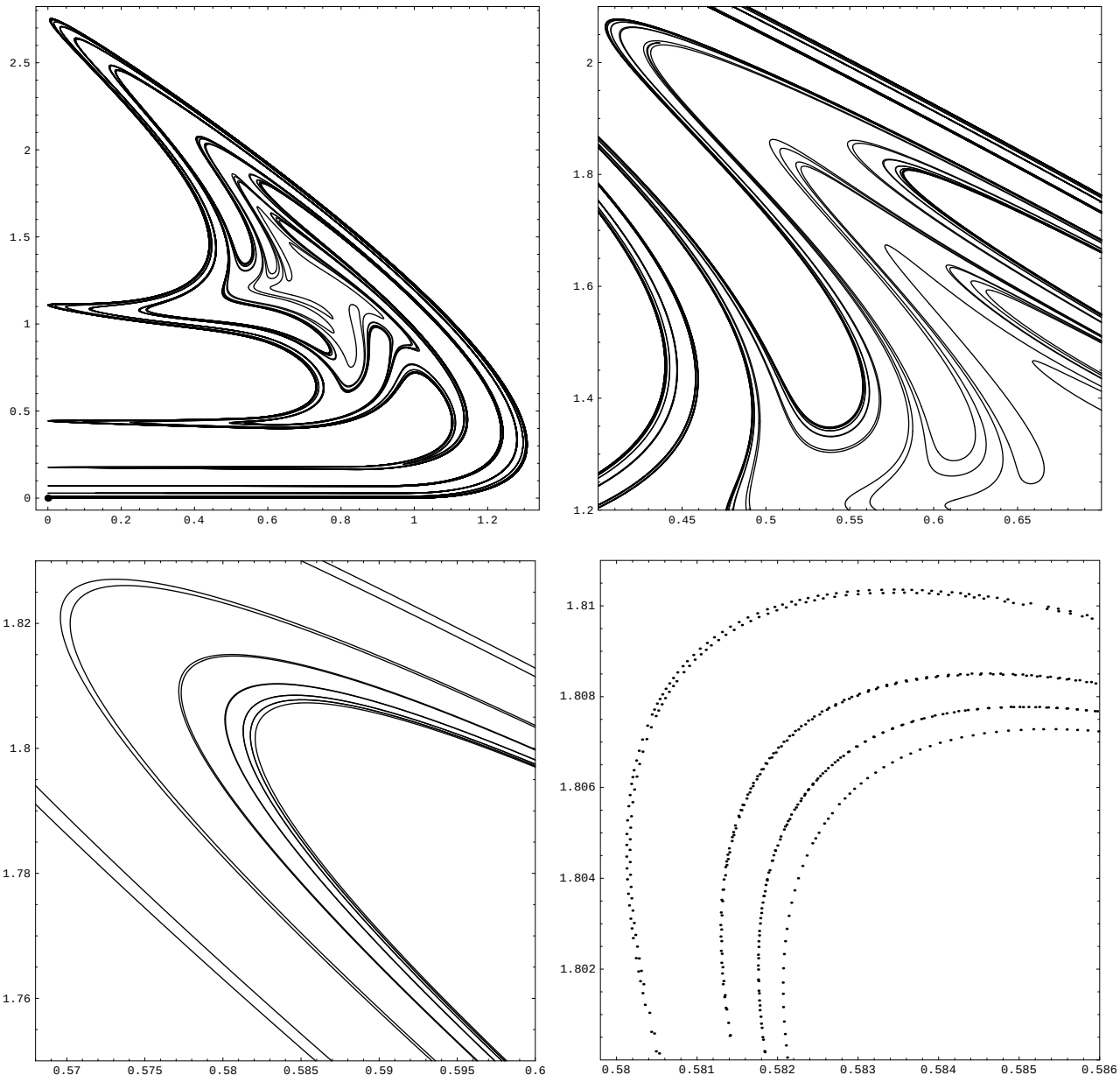

Figure 7: *Zooming into* $W^u(\mathbf{0})$ *at the tangency of the shear map, with the distribution of the computed points (lower right).* ($c = 0.811580$*; branch of* $W^u(\mathbf{0})$ *computed up to arclength 500.)*

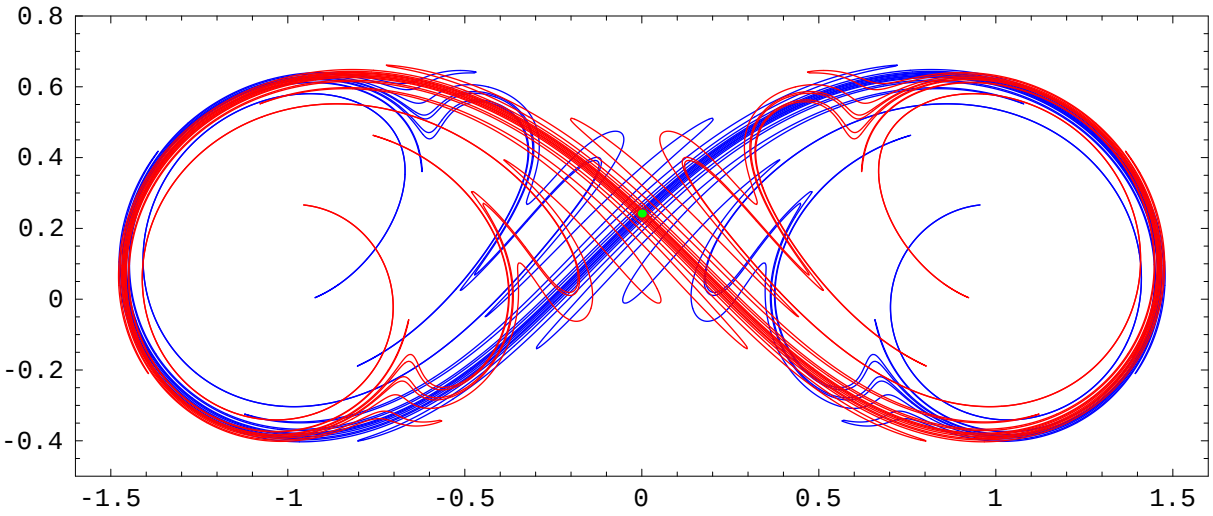

Figure 8: *Homoclinic tangle of the conservative IBV map with the same direction of rotation. ($b_1 = b_2 = 1$, $\mu_1 = \mu_2 = 0.25$; all branches computed up to arclength 50.)*

3.2 The IBV map

Inspired by the work in [1, 12, 22], we consider a planar map, which we call the *IBV map*, modeling two independent blinking vortices in an infinitely large container of fluid (with possible injection or drainage of fluid at the vortices). The IBV map is most conveniently written as a map of the complex plane $\mathbb{C}$. A vortex at the origin is described by the map

$$R_{\mu,b}(z) = \; b \; \exp(\; 2\pi i \frac{\mu}{|z|^2} \;),$$

where μ specifies the amount of rotation at the unit circle, and $b \in (0, \infty)$ models injection or drainage of fluid. The IBV map is now obtained by considering two independent vortices v_1 at $+1$ and v_2 at -1. To obtain a formula, we first shift the point v_1 to the origin, apply a vortex map, shift the point v_2 to the origin, apply another vortex map, and finally shift the origin back to v_2. In other words, the IBV map is the diffeomorphism

$$\Phi_{\mu_1,b_1,\mu_2,b_2} = T_{-1} \circ R_{\mu_1,b_1} \circ T_2 \circ R_{\mu_2,b_2} \circ T_{-1}, \tag{5}$$

where $T_c(z) = z + c$ is the translation by c. This map depends on four real parameters and has rich dynamics. The conservative case ($b_1 = b_2 = 1$)

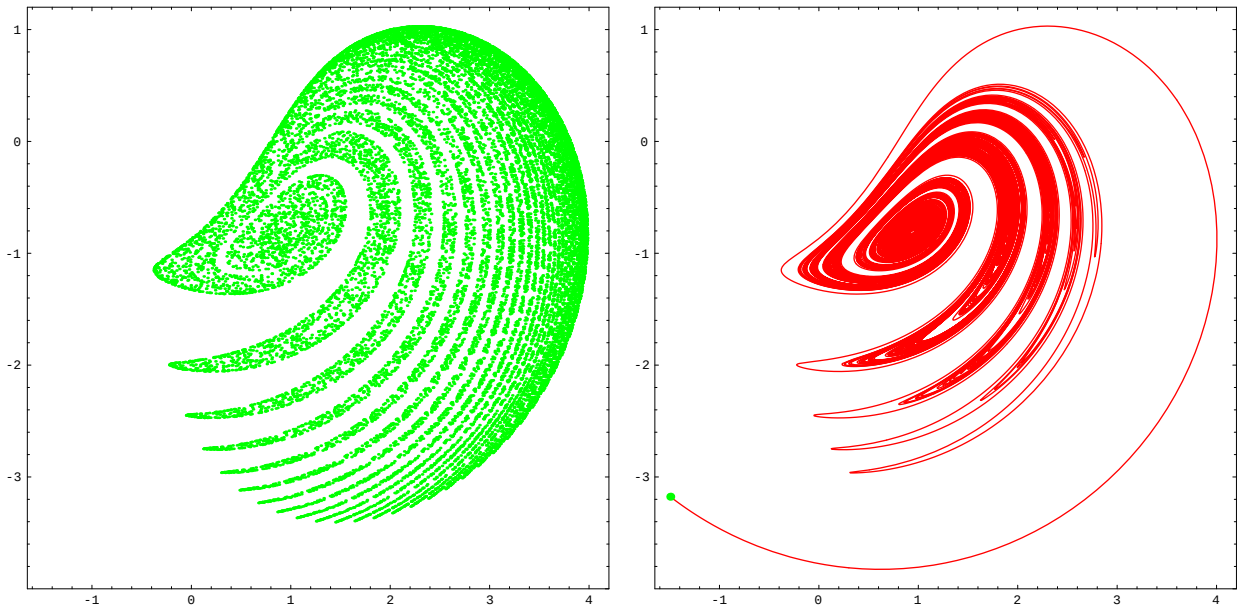

Figure 9: *The strange attractor (left) of the dissipative IBV map with opposite directions of rotation attracts one branch of the unstable manifold of a fixed point (right). ($b_1 = 0.9$, $b_2 = 1.05$, $\mu_1 = -\mu_2 = 0.25$; branch of $W^u(z_0)$ computed up to arclength 10,000.)*

with the same direction of rotation ($\mu_1 = \mu_2$) reduces to the blinking vortex map of Aref [1, 12]. The map studied in [22] can be interpreted as the limit $\mu_1, \mu_2 \to 0$ in a rescaled neighborhood of one of the vortices. Note that the map Φ also allows to consider the case of counter-rotating vortices ($\mu_1 = -\mu_2$), which does not seem to have been studied. The properties of the IBV map will be discussed elsewhere. It is used here for testing purposes because of its strong recursive spiraling.

First we consider an example of the conservative case of co-rotating vortices studied in [1, 12]. We set $b_1 = b_2 = 1$ and $\mu_1 = \mu_2 = 0.08$, for which Φ has the saddle point $z_0 \approx 0.241988\, i$. Its stable and unstable manifolds, both computed up to arclength 50, form the homoclinic tangle shown in Fig. 8. Note that, by virtue of the map, the unstable manifold is the image of the stable manifold under the symmetry transformation $z \mapsto -z$. The chosen accuracy is $\alpha_{\min} = 0.2$, $\alpha_{\max} = 0.3$, $(\Delta\alpha)_{\min} = 10^{-5}$, $(\Delta\alpha)_{\max} = 10^{-4}$ and $\Delta_{\min} = 5 * 10^{-3}$.

As a second example we choose a case of counter-rotating vortices with injection and drainage, namely $b_1 = 0.9$, $b_2 = 1.05$ and $\mu_1 = -\mu_2 = 0.25$. Then Φ has the strange attractor shown in Fig. 9 (left). It has been obtained with DsTool [2] by recording 20,000 iterates after disregarding a sufficiently long transient. We computed one branch of the unstable manifold of the saddle point $z_0 \approx -1.49477 - 3.17655\,i$ up to an arclength of 10,000. To keep the amount of data manageable we used the relatively low accuracy of $\alpha_{\min} = 0.2$, $\alpha_{\max} = 0.3$, $(\Delta\alpha)_{\min} = 10^{-3}$, $(\Delta\alpha)_{\max} = 10^{-2}$ and $\Delta_{\min} = 5 * 10^{-3}$, which resulted in a total of 289,594 mesh points. The manifold is shown in Fig. 9 (right). While it is attracted to the strange attractor it spirals repeatedly and recursively into the center of the picture, before making spiraling excursions into the 'fingers'. This is why a very long piece of the manifold is needed in order to see excursions to the fourth finger. By comparing the two panels of Fig. 9 one gets an idea of the accuracy of the computation: indeed the tips of the 'fingers' coincide. This is quite remarkable, given the arclength of the manifold that is required to reach the tip of the fourth 'finger'.

3.3 The driven-damped pendulum

To demonstrate the performance of our algorithm for Poincaré maps of vector fields we consider the driven-damped pendulum, given as the non-autonomous vector field

$$\begin{aligned} \dot{p} &= q \\ \dot{q} &= -\omega^2 \sin p - c\,q + A\cos(\Omega\,t)\ . \end{aligned} \tag{6}$$

Here ω is the frequency of the (linearized) pendulum, c is the damping, Ω is the frequency of the forcing, and A is its amplitude. For a periodically forced system like (6), the Poincaré map P is simply the (stroboscopic) time $2\pi/\Omega$ map of the flow. It lives on the cylinder $\mathbb{R}/2\pi\mathbb{Z} \times \mathbb{R}$, with the covering space $\mathbb{R} \times \mathbb{R}$ given by the (p, q)-plane.

It is well-known that P can exhibit complicated dynamics. We consider the particular choices of the parameters $\omega = 2.5$, $c = 0.5$, $\Omega = 1.5$ and $A = 4.0$, for which one finds the strange attractor shown in Fig. 10 (left). It has been obtained with DsTool [2] by recording 10,000 iterates after disregarding a sufficiently long transient. The points were then projected onto a planar

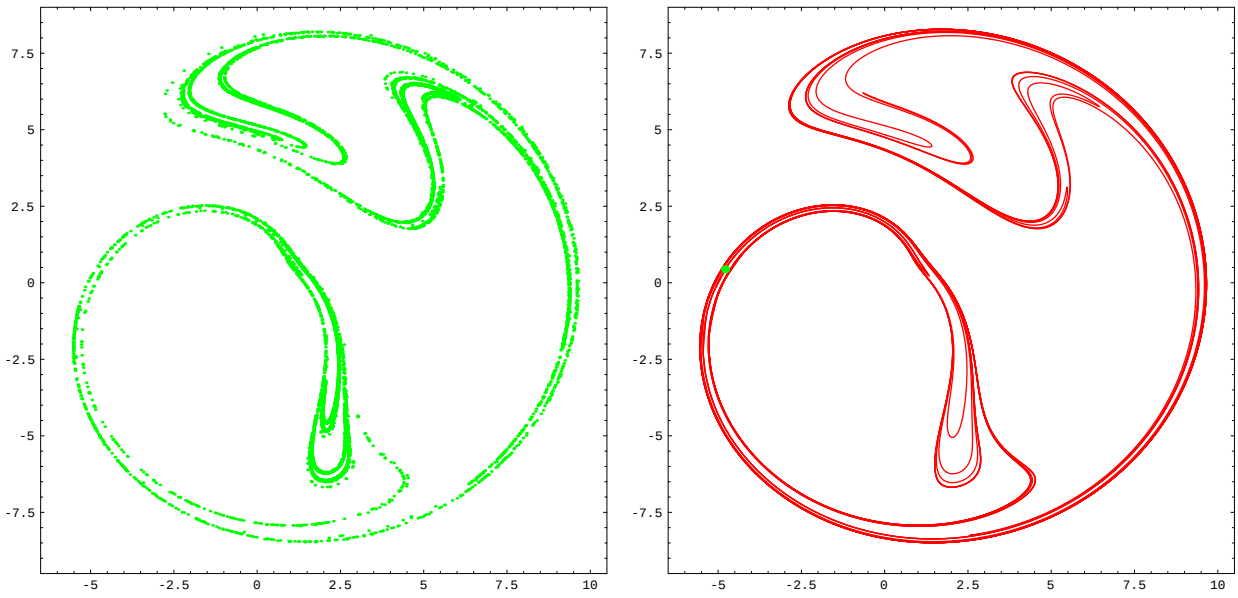

Figure 10: *The strange attractor (left) for the driven-damped pendulum attracts the unstable manifold of a fixed point (right). ($\omega = 2.5,\ c = 0.5,\ \Omega = 1.5,\ A = 4.0$; both branches of $W^u(x_0)$ computed up to arclength 300.)*

annulus by the coordinate change

$$\begin{pmatrix} x \\ y \end{pmatrix} = \begin{pmatrix} (q-L)\cos p \\ (q-L)\sin p \end{pmatrix}, \tag{7}$$

where we choose $L = -4$; L is a lower bound for the q-values of the object of interest.

For the chosen parameters the point $x_0 \approx (3.0502, 0.8128)$ is a saddle point, and it seems to lie on the attractor. Figure 10 (right) shows the two branches of $W^u(x_0)$, each up to arclength 300. The computation has been performed in the covering space $\mathbb{R} \times \mathbb{R}$, and then the result was transformed onto the plane by (7). The accuracy of the computation was $\alpha_{\min} = 0.2,\ \alpha_{\max} = 0.3,\ (\Delta\alpha)_{\min} = 10^{-4},\ (\Delta\alpha)_{\max} = 10^{-3}$ and $\Delta_{\min} = 5{*}10^{-3}$, which resulted in a total of 17,067 points along the manifold.

We also computed both branches of the stable manifold $W^s(x_0)$ up to arclength 300 with the same accuracy. It is interesting to see how the two manifolds $W^u(x_0)$ and $W^s(x_0)$ intersect in the covering space $\mathbb{R} \times \mathbb{R}$; see Fig. 11.

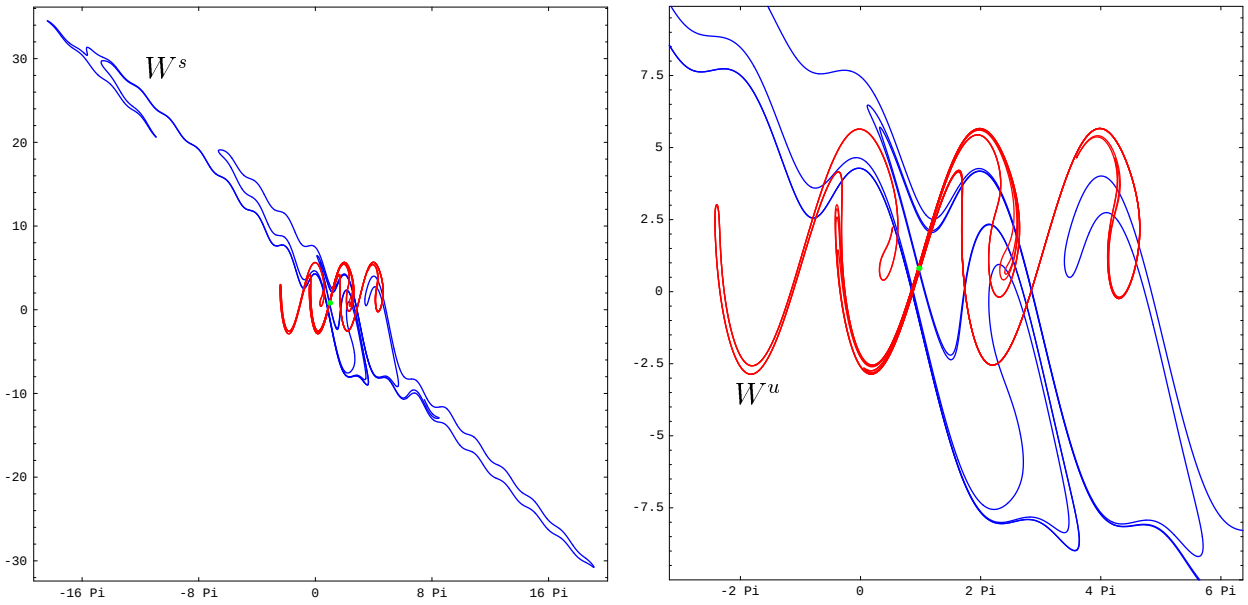

Figure 11: *Stable and unstable manifolds of a fixed point for the driven-damped pendulum on the covering space* $\mathbb{R}^2$ *(left), and enlargment (right). (*$\omega = 2.5,\ c = 0.5,\ \Omega = 1.5,\ A = 4.0$*; all branches computed up to arclength 300.)*

Acknowledgments

B.K. is grateful for the hospitality and financial support of the Institute of Mathematics and its Applications and The Geometry Center, Minneapolis. H.O. thanks the Vrije Universiteit Amsterdam for its hospitality.

References

[1] H. Aref, "Stirring by chaotic advection", *J. Fluid Mech.* **143**:1–21, 1984.

[2] A. Back, J. Guckenheimer, M.R. Myers, F.J. Wicklin, and P.A. Worfolk, "DsTool: Computer assisted exploration of dynamical systems", *Notices Amer. Math. Soc.* **39**(4):303–309, 1992.

[3] M. Dellnitz and A. Hohmann, "The computation of unstable manifolds using subdivision and continuation", in H.W. Broer et al. (eds.), *Progress in Nonlinear Differential Equations and Their Applications* **19**:449–459, Birkhäuser Verlag, Basel / Switzerland, 1996.

[4] M. Dellnitz and A. Hohmann, "A subdivision algorithm for the computation of unstable manifolds and global attractors", *Num. Math.* **75**:293–317, 1997.

[5] C. Grebogi, E. Ott and J.A. Yorke, "Crises, sudden changes in chaotic attractors, and transient chaos", *Physica D* **7**:181–200, 1983.

[6] J. Guckenheimer and P. Holmes, *Nonlinear Oscillations, Dynamical Systems, and Bifurcations of Vector Fields*, Springer, second printing, 1986.

[7] S.M. Hammel, C.K.R.T. Jones annd J.V. Moloney, "Global dynamical behavior of the optical field in a ring cavity", *J. Opt. Soc Am. B* **2**(4):552–564, 1985.

[8] M. Hénon, "A two-dimensional mapping with a strange attractor", *Comm. Math. Phys.* **50**:69–77, 1976.

[9] D. Hobson, "An efficient method for computing invariant manifolds of planar maps", *J. Comput. Phys.* **104**(1):14–22, 1993.

[10] A.J. Homburg, D. Sands, and R. de Vilder, "Computing invariant sets", Technical Report 57/96, Schwerpunktprogramm Danse der DFG, 1996.

[11] K. Ikeda, H. Daido and O. Akimoto, "Optical turbulence: chaotic behavior of transmitted light from a ring cavity", *Phys. Rev. Lett.* **45**(9):709–712, 1980.

[12] D.V. Khakhar, H. Rising and J.M. Ottino, "Analysis of chaotic mixing in two model systems", *J. Fluid Mech.* **172**:419–451, 1986.

[13] B. Krauskopf and H.M. Osinga, *Globalizing two-dimensional unstable manifolds of maps*, to appear in Int. J. Bifurcation & Chaos, 1997.

[14] H.E. Nusse and J.A. Yorke, "A procedure for finding numerical trajectories on chaotic saddles", *Physica D* **36**:137–156, 1989.

[15] H.M. Osinga, *Computing invariant manifolds: Variations on the graph transform*, PhD thesis, Groningen University, 1996.

[16] G. Osipenko and S. Campbell, "Applied symbolic dynamics: attractors and filtrations", in preparation.

[17] J. Palis and W. de Melo, *Geometric Theory of Dynamical Systems*, Springer, 1982.

[18] J. Palis and F. Takens, *Hyperbolicity & sensitive chaotic dynamics at homoclinic bifurcations*, Cambrigde University Press, 1993.

[19] T.S. Parker and L.O. Chua, *Practical Numerical Algorithms for Chaotic Systems*, Springer, 1989.

[20] W.H. Press, S.A. Teukolsky, W.T. Vetterling, and B.P. Flannery, *Numerical Recipes in C: the Art of Scientific computing*, Cambridge University Press, 2 edition, 1992.

[21] C. Simó, "On the analytical and numerical approximation of invariant manifolds", in D. Benest and C. Froeschlé (eds), *Les Méthodes Modernes de la Mécanique Céleste*, pages 285–329, Goutelas, 1989.

[22] G. Stolovitzky, T.J. Kaper and L. Sirovich, "A simple model of chaotic advection and scattering", *Chaos* **5**(4):671–686, 1995.

[23] Z. You, E.J. Kostelich, and J.A. Yorke, "Calculating stable and unstable manifolds", *Int. J. Bifurcation & Chaos* **1**(3):605–623, 1991.